Optics Communications 285 (2012) 315–321

Contents lists available at SciVerse ScienceDirect

Optics Communications

journal homepage: www.elsevier.com/locate/optcom

Spectroscopy and efficient laser emission of Yb^{3+}: LuAG single crystal grown by μ-PD

S. Veronesi [a,*], Y.Z. Zhang [a], M. Tonelli [a], A. Agnesi [b], A. Greborio [b], F. Pirzio [b], G. Reali [b]

[a] NEST Istituto Nanoscienze-CNR and Dipartimento di Fisica, Università di Pisa, Largo B. Pontecorvo 3, IT-56127 Pisa, Italy
[b] Dipartimento di Elettronica dell'Università di Pavia, Via Ferrata 1, IT-27100 Pavia, Italy

ARTICLE INFO

Article history:
Received 22 July 2011
Received in revised form 30 August 2011
Accepted 13 September 2011
Available online 29 September 2011

Keywords:
Optical materials
Crystal growth
Optical properties
IR laser emission
Diode pumped
Ytterbium

ABSTRACT

A LuAG shaped rod crystal, doped with Yb^{3+}, has been grown by μ-PD technique. The crystal diameter was about 3 mm and the length around 130 mm. A complete spectroscopic investigation in the temperature range 10–300 K is reported and data has been utilized to model the laser behavior. In the laser experiment the Yb:LuAG sample was placed in an X cavity and pumped longitudinally obtaining an efficient CW laser emission. The Yb:LuAG laser yielded a maximum output power of 23 mW with a slope efficiency of 32% and a threshold around 35 mW, at lasing wavelength of 1030 nm. No significant depolarization effects were observed, indicating a crystal growth with negligible stress. The output beam profile was investigated, yielding $M^2 \approx 1.0$ in both directions, further confirming the good optical quality of the sample.

1. Introduction

The development of lasers in the near infrared region, in particular around 1 μm, started long time ago and at present the market offers devices to fulfill any research or industrial needs. Nevertheless the research for new materials or new ways to realize old ones is still running. The most popular and diffuse devices are Yb^{3+} and Nd^{3+} based laser, and the most used host is largely YAG. It has a cubic crystal structure and it exhibits good thermal conductivity (10.7 $Wm^{-1}K^{-1}$) but it decreases, increasing the doping level. This behavior could be problematic in high power applications even if power as high as 1 kW [1] has been obtained. An interesting option to YAG is LuAG, which has a lower thermal conductivity (8 $Wm^{-1}K^{-1}$) but almost independent from the doping level, in contrast with the decreasing one of YAG; the LuAG hardness in Moh's value is 8.5. This feature makes LuAG an appealing material for high power laser applications. For this reason a fast and cheap route to obtain laser grade LuAG single crystal could represent the starting point for an upgrade of the current technology based on YAG host. In the present work we report on the laser emission and spectroscopic investigation of a LuAG:Yb^{3+} crystal, grown by micro-pulling down (μ-PD) technique. This is not the first laser emission [2] obtained with a LuAG sample coming from μ-PD technique, but our sample demonstrates more efficient laser performances, as discussed in the following. In particular, we intended to assess the intrinsic optical quality of the crystal, therefore we employed low-power pumping in order to discern crystal flaws from possible thermal effects showing up at higher excitation levels. The μ-PD technique has demonstrated to be useful in developing fiber or rod shaped crystals suitable to be easily used in a laser cavity [3,4,5,6,7]. We want to underline that utilizing this technique it is possible to grow fibers with diameter as low as 500 μm, that cannot be obtained from massive boules, allowing a more effective cooling in high power applications. Moreover all the raw material loaded in the crucible can be utilized in the crystal growth and it is possible to load very small amount of raw material to grow small sample in an optimizing feedback loop. So μ-PD represents a cheap and relatively fast way to grow this or other hosts in developing laser grade materials, not necessarily as long fiber-like monocrystals or minirods, but also in smaller pieces usually employed in low-power microchip and ultrafast laser oscillators.

2. Crystal growth and experimental setup

2.1. Crystal growth

The sample under investigation was a LuAG single crystal doped with 1%.at Yb^{3+} concentration which has been grown from an oriented seed. The growth was performed in the NEST laboratories, that are equipped with a homemade μ-PD furnace with RF heating. LuAG is a rare-earth garnet, having a cubic crystal structure (space group O_h^{10}-*Ia3d*) with lattice parameter a = 11.906 [8]. The rare earth trivalent ions normally fill the dodecahedral lattice sites, with a negligible fraction of octahedral occupation at low doping levels [9]. Special care has been devoted to the quality of vacuum system, which has an ultimate pressure better than 10^{-7} mbar and the growth process was carried out in a high-purity (99.999%) argon atmosphere. The powders, from AC materials (Tarpon Springs, Fl., USA) had 5 N purity and the sample

* Corresponding author. Tel.: +39 050 2214 184; fax: +39 050 2214 333.
E-mail address: veronesi@df.unipi.it (S. Veronesi).

0030-4018/$ – see front matter © 2011 Elsevier B.V. All rights reserved.
doi:10.1016/j.optcom.2011.09.032

was grown starting from Lu_2O_3 and Al_2O_3 as raw material and a proper amount of Yb_2O_3 powder. Growing has been performed in an Iridium crucible with a bottom tip of 3 mm diameter and an orifice of 0.5 mm. During growth the pulling rate was about 0.3 mm/h, and the temperature of the melt was about 2350 K. The average size of the LuAG crystal, shown in Fig. 1, was about 3.02 ± 0.04 mm in diameter and 130 mm in length. The crystal has been annealed at 1700 K in air in order to oxide the Yb^{2+} ions, that are usually present in the as grown sample and give it a bluish color, to Yb^{3+}. The optical quality of the grown crystal has been checked observing the transmission of a He–Ne TEM_{00} laser beam, demonstrating the absence of macroscopic defects (see Results and discussion section). From the rod, two samples were prepared, one for the laser experiment and another for spectroscopic measurements.

2.2. Spectroscopy

Room temperature absorption measurements were performed by a CARY 500 spectrophotometer in the range 300–2000 nm with a resolution of 1 nm, in order to check the absorption lines of the Yb^{3+} and also to verify the absence of lines belonging to pollutants or Yb^{2+} ions. We recorded a detailed spectrum from 800 to 1100 nm relative to the $^2F_{7/2} \rightarrow {}^2F_{5/2}$ laser transition with a resolution of 0.6 nm. The fluorescence measurements have been performed by exciting the sample with a near infrared laser diode tuned at 980 nm, according to the absorption spectrum of LuAG:Yb^{3+}. The sample was placed inside a CTI CRYOGENICS helium cryo-cooler which allows measurements in the range 10–300 K. The laser beam was focused onto the sample by means of a 10 cm focal length lens. The fluorescence was collected by a 7.5 cm focal length infrasil lens, perpendicularly with respect to the excitation beam in order to minimize pump spurious scattering collection. Luminescence was focused on the entrance slit of a 32 cm focal length Jobin-Yvon monochromator and opportunely filtered. The monochromator was equipped a 600 g/mm diffraction grating to operate in the wavelength range around 1000 nm. Signal was detected by an InSb detector, cooled to the liquid nitrogen temperature and acquired by a SR830 Lock-in Amplifier. The resolution of the fluorescence spectra was 2.5 nm in the range 870–1080 nm. The acquired spectra were normalized for the optical response of the system using a black-body source at 3000 K. Levels lifetime were measured by means of a pulsed tunable Ti:Al_2O_3 laser with a 10 Hz repetition rate and 30 ns pulse width. In all lifetime measurements the pulse energy was reduced as much as possible to minimize power dependent effects. The exciting beam was properly attenuated to avoid radiation trapping that affect the lifetime of the $^2F_{5/2}$ manifold, moreover the laser beam was focused near the edge of the crystal utilized for light collection. To prevent the detection of scattered laser light, the collected radiation was suitably filtered. Signal was detected by an InSb detector, cooled to the liquid nitrogen temperature and amplified, with an overall response time of about 3 μs. Data acquisition was performed with a digital oscilloscope connected to a computer.

2.3. Laser

The experimental setup is depicted in Fig. 2. The pump diode was a single-mode 300-mW laser diode (FLC GmbH), emitting at 935 nm with a narrow single-longitudinal and single-spatial mode with 50 pm linewidth. The pump radiation was collimated with a 0.4 NA, 6.24 mm focal length aspheric lens. A pair of anamorphic prisms

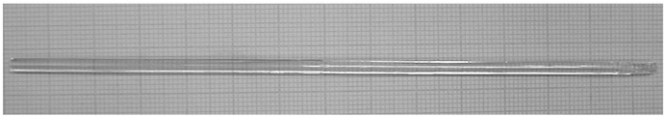

Fig. 1. LuAG fiber after the annealing at 1700 K.

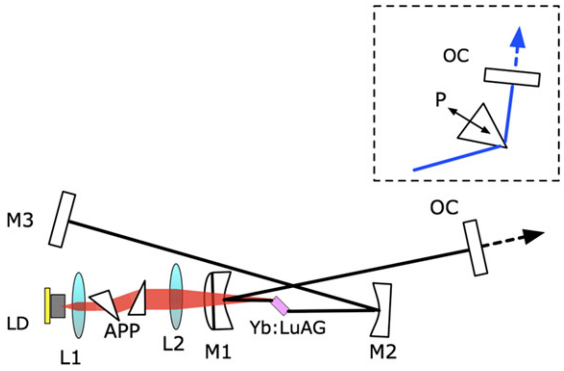

Fig. 2. Resonator layout. LD: pump laser diode; L_1: aspheric lens (6.5-mm focal, NA 0.4); APP: anamorphic N-SF11 prisms pair; L_2: spherical singlet lens (100-mm focal); M_1: concave mirror, 50 mm curvature, high-reflectivity (HR) at 1000–1100 nm, high-transmissivity at 900–950 nm; M_2: concave mirror, 100 mm curvature, HR; M_3: flat mirror: HR; OC: output coupler, 30′ wedge. In the Inset: P: SF10 prism; OC: output coupler.

was employed to reshape the elliptical pump beam, and a 100 mm spherical singlet lens was used to eventually focus the pump into the active medium. The maximum power delivered to the laser crystal was 270 mW. A CCD camera was employed to characterize the pump beam profile in the focal region of the optical system yielding waist radii $w_{px} \times w_{py} = 25 \times 25\ \mu m^2$ in air and beam quality parameters $M_x^2 = 1.2$ and $M_y^2 = 1.2$. The resonator beam waist radius was calculated to be 15–20 μm within the stability range. The pump spot dimensions were optimized in order to both ensure a reasonable mode-matching with the resonant beam and a pump beam confocal parameter comparable with the length of the active medium, to minimize the effect of the reabsorption losses in the quasi-three-level active medium. The Yb:LuAG laser crystal was a 4.5 mm long, 1%-doped rod, with a diameter of 3 mm. The active medium was contacted to a metallic plate, without any active cooling, and oriented at the Brewster angle in order to minimize insertion losses. In order to compensate for cavity mode astigmatism, M_1 and M_2 folding angles were set to about 7°, whereas the separation between M_1 and M_2 was chosen to be ≈86 mm in order to operate the resonator near the center of its stability range. The M_2–M_3 and M_1-OC cavity arms length was about 260 and 350 mm, respectively. In order to make a significant comparison, a commercial 10%-doped, 1 mm thin Yb:YAG crystal grown by Czochralski method was also characterized with the same laser setup, with a pump focusing lens of 75 mm focal length, yielding a pump spot inside the active medium of about $w_{px} \times w_{py} \approx 20 \times 20\ \mu m^2$. This optimized the performance of the thinner Yb:YAG sample, better matching its shorter absorption length with the confocal parameter. Unfortunately, Yb:LuAG crystals grown by traditional techniques were not readily available for a more straightforward comparison.

3. Results and discussion

The optical quality of the crystal has been checked measuring the distortions caused by the sample on the propagation of a TEM_{00} helium neon laser beam. The TEM_{00} mode was selected by using a pinhole and the outcoming beam dimensions were regulated with an iris diaphragm in order to obtain a spot slightly smaller than the sample diameter. The beam intensity profile was acquired with a CCD camera equipped with proper imaging lenses. In Fig. 3a it is possible to observe the intensity profile of the beam, and the diffraction pattern produced by the iris is well evident. In Fig. 3b the intensity profile obtained inserting a LuAG sample on the laser beam without changing the other experimental conditions is shown. The intensity profile confirms the absence of significative defects inside the sample.

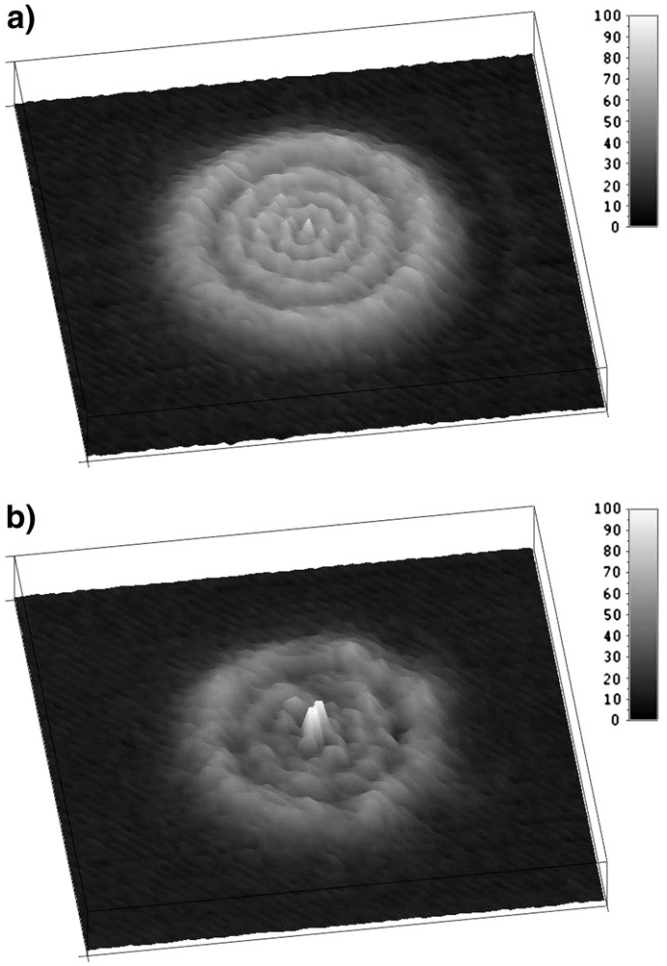

Fig. 3. a) Helium–Neon laser beam image without the LuAG sample. The diffraction pattern produced by the iris is well evident. b) Laser beam image propagated through the LuAG sample.

3.1. Spectroscopy

Absorption measurements: The absorption measurements have been performed at room temperature with non polarized light, due to crystal isotropy. A first spectrum has been recorded in the range 300–2000 nm, with a lower resolution, in order to check the absence of residual Yb^{2+} bands and of possible pollutants. After this check a second detailed spectrum was acquired in the range 800–1100 nm, with higher resolution, to determine the Yb^{3+} absorption lines relative to the $^2F_{7/2} \rightarrow {}^2F_{5/2}$ transition, and to check the doping level. In Fig. 4 the absorption spectrum is shown, the most intense absorption peak corresponds to the zero phonon line and lies at 968.4 nm with a $\alpha_M = 1.4\,\mathrm{cm}^{-1}$ and the absorption at pump wavelength (935 nm) was about $\alpha_P = 1.1\,\mathrm{cm}^{-1}$.

Fluorescence and lifetime measurements: Fluorescence spectra, in the range 900–1070 nm, were recorded as a function of temperature between 10 and 300 K, shown in Fig. 5. The emission peaks show a small red shift as temperature increases toward 300 K, and from the spectra it is possible to evaluate an emission peaks shift of 1.4 pm/K in general agreement with the literature value of 4 pm/K obtained for a different system (Nd:YAG) [10]. Lifetime measurements, in the range 10–300 K, have been performed exciting the sample with a pulsed tunable $Ti:Al_2O_3$ laser as previously described. The careful choice of exciting power allows us to avoid radiation trapping effects within the experimental errors. The decay curve shows a single exponential behavior and the lifetime value of the $^2F_{5/2}$ manifold was independent on the temperature with an average value of 1.03 ± 0.02 ms.

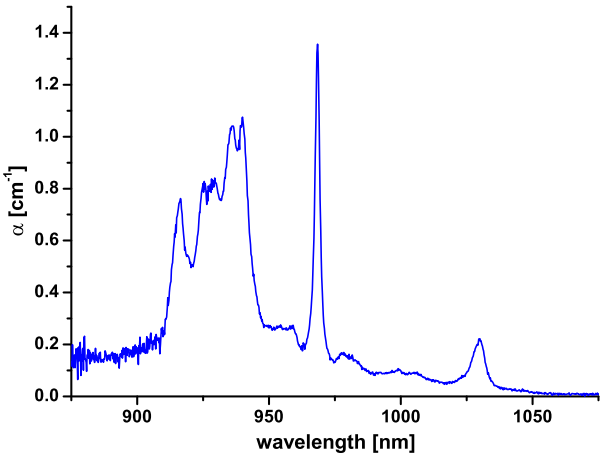

Fig. 4. Room temperature Absorption spectrum for LuAG: 1 at.% Yb^{3+} relative to the transition $^2F_{7/2}\nu \rightarrow {}^2F_{5/2}$.

Measured lifetime is in agreement with literature values [9,11]. In order to evaluate the laser performances the emission cross section, utilizing the $\beta-\tau$ method, and absorption cross section have been calculated. The behavior agrees with that reported in literature [9,11] and it is shown in Fig. 6.

3.2. Laser

Model for the quasi-three levels laser. Quite general, space-dependent models of quasi-three levels lasers by Fan et al. [12] and Risk [13] yield accurate predictions in most situations. However, they require a minimum of numerical approach and are usually applied to lasers operating at a precise wavelength, for which generally the degeneracy factors and the occupation probabilities of the sublevels are known quantities. Here we use a simpler approach, still valid in many instances, which leads to explicit relationships (output vs. input power, threshold pump power), providing a different insight into the physics of Yb and quasi-three levels Nd solid-state lasers. Let us consider the dynamics of the lower and upper multiplets, assuming fast internal thermalization, with reference to Fig. 7:

$$\frac{dn_1}{dt} = \frac{n_2}{\tau_f} + \frac{\sigma_e(\lambda_L) I_L n_2}{h\nu_L} + \frac{\sigma_e(\lambda_P) I_P n_2}{h\nu_P} - \frac{\sigma_a(\lambda_L) I_L n_1}{h\nu_L} - \frac{\sigma_a(\lambda_P) I_P n_1}{h\nu_P} \quad (1)$$

$$n = n_1 + n_2. \quad (2)$$

The spectroscopically measurable cross section spectra are especially useful when studying tunable lasers, since wavelength-

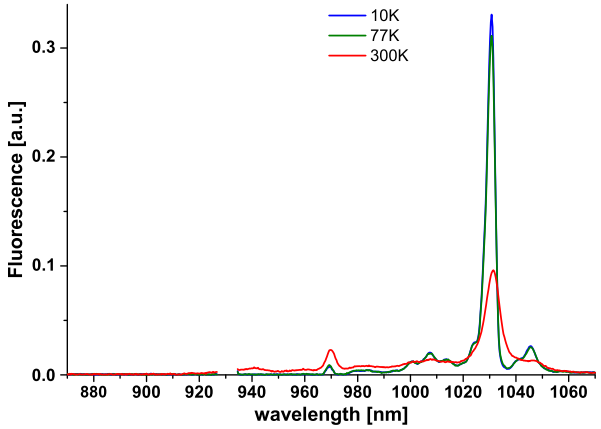

Fig. 5. Fluorescence as a function of temperature for $^2F_{5/2}$ manifold of Yb^{3+} in LuAG.

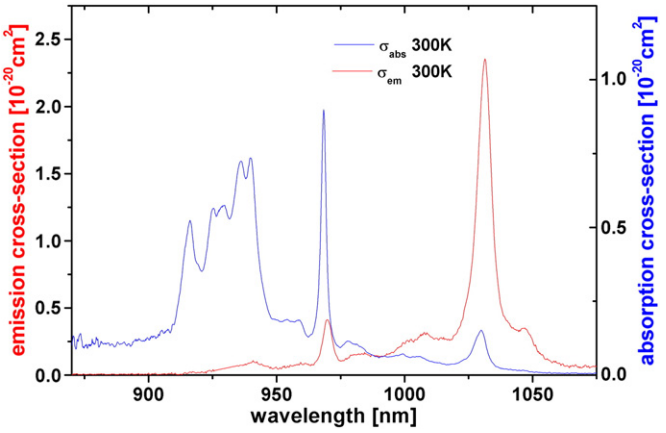

Fig. 6. Room temperature emission and absorption cross section of Yb^{3+} in LuAG.

dependent parameters such as laser threshold and laser output can be readily calculated, as it will be shown. As a more compact notation we define $\sigma_e(\lambda_L)=\sigma_{eL}$ etc. The gain coefficient g clearly depends on emission and absorption cross sections in the wavelength range of interest for laser operation:

$$g=\sigma_{eL}n_2-\sigma_{aL}n_1. \tag{3}$$

Most often the parameter $\beta=n_2/n$ defines the fraction of ion population excited into the upper multiplet. The transparency condition requires a pump intensity

$$I_{PT}(\lambda_L,\lambda_P)=\frac{h\nu_P}{\tau_f}\frac{1}{\frac{\sigma_{aP}\sigma_{eL}}{\sigma_{aL}}-\sigma_{eP}}. \tag{4}$$

From Eq. (1) at the steady state we can determine n_2:

$$n_2=\frac{\left(\frac{\sigma_{aL}}{\sigma_{aL}+\sigma_{eL}}\frac{I_L}{I_{SL}}+\frac{\sigma_{aP}}{\sigma_{aP}+\sigma_{eP}}\frac{I_P}{I_{SP}}\right)}{1+\frac{I_L}{I_{SL}}+\frac{I_P}{I_{SP}}}n \tag{5}$$

where we defined the laser and pump saturation intensity, respectively:

$$I_{SL}=\frac{h\nu_L}{(\sigma_{aL}+\sigma_{eL})\tau_f}\qquad\text{and}\qquad I_{SP}=\frac{h\nu_P}{(\sigma_{aP}+\sigma_{eP})\tau_f}. \tag{6}$$

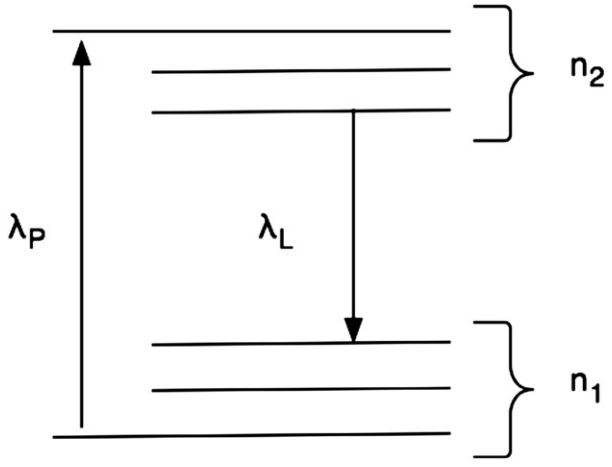

Fig. 7. Laser level scheme.

In order to simplify the analysis, let us assume that the lower multiplet is not depleted significantly: $I_P<<I_{SP}$. This assumption must be checked for each parameter set, however since $I_{PT}<<I_{SP}$, it is likely that the "small population depletion" approximation holds unless very strong pumping is used. Laser oscillation occurs at unit loop gain, that is:

$$2\int_0^{l_g}(\sigma_{eL}n_2-\sigma_{aL}n_1)dz=L+T \tag{7}$$

$$2\int_0^{l_g}(\sigma_{eL}+\sigma_{aL})n_2dz-2\int_0^{l_g}\sigma_{aL}ndz=L+T \tag{8}$$

where l_g is the crystal length.

According to the assumption of small depletion of the lower multiplet, the term

$$\delta=2\int_0^{l_g}(\sigma_{aL}n)dz=2\alpha_L l_g \tag{9}$$

represents the unsaturated losses at the laser wavelength (α_L is the absorption coefficient at λ_L):

$$2\int_0^{l_g}\frac{\left(\sigma_{aL}\frac{I_L}{I_{SL}}+\sigma_{aP}\frac{\nu_L}{\nu_P}\frac{I_P}{I_{SL}}\right)}{1+\frac{I_L}{I_{SL}}}ndz=L+T+\delta. \tag{10}$$

Assuming small coupling T and parasitic losses L (even though up to few 10% still yield acceptable errors), the laser intensity in the crystal does not change appreciably:

$$\frac{\delta\frac{I_L}{I_{SL}}}{1+\frac{I_L}{I_{SL}}}+2\frac{\int_0^{l_g}\frac{\lambda_P}{\lambda_L}\frac{\alpha_P I_P}{I_{SL}}dz}{1+\frac{I_L}{I_{SL}}}=L+T+\delta. \tag{11}$$

Indeed, if $I_P<<I_{SP}$ we obtain $\alpha_P=(\sigma_{aP}n_1-\sigma_{eP}n_2)=\sigma_{aP}n-(\sigma_{aP}+\sigma_{eP})n_2\approx\sigma_{aP}n$ since well above laser threshold one can verify from Eq. (5) that $n_2<<n$. Being $dP_{abs}/dz=\alpha_P P_P$, defining $P_{SL}=I_{SL}A$ (A is the pump and laser beam cross section) and considering the standing wave effect doubling the intracavity intensity at any longitudinal position:

$$\frac{\delta\frac{2P_L}{P_{SL}}}{1+\frac{2P_L}{P_{SL}}}+2\frac{\frac{\lambda_P}{\lambda_L}\frac{P_{abs}}{P_{SL}}}{1+\frac{2P_L}{P_{SL}}}=L+T+\delta. \tag{12}$$

Eventually, we can solve for the output power $P_o=P_L T$:

$$P_o=\frac{\lambda_P}{\lambda_L}\frac{T}{L+T}\left[P_{abs}-P_{abs,th}\right] \tag{13}$$

$$P_{abs,th}=\frac{P_{SL}}{2}\frac{\lambda_L}{\lambda_P}(L+T+\delta). \tag{14}$$

Considering the initial assumptions, this result is identical to that for the four-level laser, for example according to the derivation outlined in Koechner's book [14]. Most remarkable is the fact that the pump threshold is settled by the reabsorption term δ, whereas this does not appear to affect the coupling efficiency and the slope efficiency, even though this might be even larger than practical values of T, as it happens for Yb:YAG lasers at their peak transition near 1030 nm. The physical explanation is that above laser threshold the oscillating field saturates such reabsorption losses, allowing in principle quantum-limited slope efficiency approaching unity for very small quantum defects. Notice that both Eqs. (13) and (14) yield results which implicitly take into account the wavelength dependence of cross sections. Finally, we note that this model includes the ideal four-level laser as a particular case. Another remarkable difference, compared with the four-levels system, is the change in the

absorbed pump power fraction above laser threshold. The pump power distribution along the longitudinal z coordinate follows the law

$$\frac{dP_P}{dz} = -(\sigma_{aP}n_1 - \sigma_{eP}n_2)P_P \tag{15}$$

which can also be recast as

$$\frac{dP_P}{dz} = -\sigma_{aP}nP_P + (\sigma_{aP}+\sigma_{eP})\frac{\frac{\sigma_{aL}}{\sigma_{aL}+\sigma_{eL}}\frac{P_L}{P_{SL}} + \frac{\sigma_{aP}}{\sigma_{aP}+\sigma_{eP}}\frac{P_P}{P_{SP}}}{1+\frac{P_L}{P_{SL}}+\frac{P_P}{P_{SP}}}nP_P. \tag{16}$$

Assuming $P_P << P_{SP}$ as before, we can readily analyze the asymptotic cases.

a) Weak pumping ($P_L = 0, P_P \to 0$):

$$\alpha_P = \sigma_{aP}n \tag{17}$$

b) Laser oscillation well above threshold, but still with small lower multiplet depletion ($P_L >> P_{SL}, P_P << P_{SP}$):

$$\alpha_P = \sigma_{aP}\left(1-\frac{\sigma_{aL}}{\sigma_{eL}}\right)n \tag{18}$$

Therefore we find that the pump absorption decreases as soon as the laser oscillation starts, since the resonant field tends to deplete the reabsorbing levels. Of course, such an effect becomes even more noticeable for zero-phonon Yb laser transitions near 980 nm, i.e. true three-level lasers for which the approximation $\sigma_{aL}/\sigma_{eL} << 1$ no longer holds and this model becomes inadequate. However, under the assumptions done, Yb lasers operating in the range 1000–1100 nm present an approximately constant pump absorption coefficient, $\alpha_P \approx \sigma_{aP}n$.

Experiment. Laser experiments in CW regime were performed employing several different output couplers (Fig. 8). A significant amount of the available pump power was not absorbed by the relatively low-doped 1% Yb:LuAG and it was transmitted through the M_2 mirror. Hence we estimated the amount of absorbed pump power by measuring the residual behind the M_2 mirror under lasing conditions. The experimental results are summarized in Fig. 8. With the optimum T = 10% output coupler (OC), at an absorbed pump power of ≈100 mW, we obtained up to 23 mW output power and ≈32% slope efficiency. We also scanned the Yb:LuAG crystal transversally with the pump beam. Accounting for good sample homogeneity, output power and general laser behavior were unaffected by the pump spot position on the crystal. Also no significant depolarization effects were observed, indicating stress-free crystal growth. We also measured the beam quality factor M^2 in the horizontal and vertical planes by scanning the beam along propagation direction in the focal plane of a spherical lens with a CCD camera, obtaining a value $M^2 \approx 1.0$ (Fig. 10). The cavity folding mirrors tilting angle was not optimized during this measurement, yielding a residual astigmatism clearly shown by the beam propagation best fit and a slight ellipticity of the spot in the focal plane (see inset of Fig. 10). However, this unoptimized working condition does not affect the beam spatial quality that confirms the good optical quality of the sample and the absence of significant thermal-induced beam distortion at these low pump levels. The lasing wavelength for any transmittance of the OC in the range 0–30% was near the main cross-section peak at 1030 nm. With the Yb:YAG crystal the optimum OC transmissivity was T = 1.6%, yielding ≈50% slope efficiency with a maximum output power of 62 mW at 158 mW of absorbed pump power (Fig. 9). The laser was operating at 1030 nm, as with Yb:LuAG. To assess the crystal loss we consider a more general expression of the total slope efficiency than in Eq. (13), including other contributions such as mode-matching efficiency and quantum efficiency in a constant η_0, also using $-ln(R)$ instead of T in a more general fashion:

$$\eta = \eta_0 \frac{\lambda_p}{\lambda_l}\frac{-ln(R)}{L-ln(R)}. \tag{19}$$

The results are summarized in Fig. 11. It turns out that the loss L for the Yb:YAG experiment is smaller than the detectable limit of the technique so we indicatively assume L≈0, whereas the Yb:LuAG shows a clear trend following Eq. (19), yielding L≈2.4%. The slight drop of slope efficiency at higher OC values for both Yb:YAG and Yb:LuAG suggests parasitic effects dependent on larger population inversion, such as upconversion. The corresponding loss per unit length in Yb:LuAG shaped rod crystal is therefore ≈0.2%/mm, in agreement with Ref. [2], and is likely due to internal scattering.

Later we inserted a SF10 dispersive prism near the OC (see inset of Fig. 2) in order to measure the output wavelength tunability in CW regime. The gain was too low in Yb:LuAG to achieve continuous tuning across an extended range, however either the main transitions of $^2F_{5/2} \to {}^2F_{7/2}$ manifolds at 1031 nm and that at 1046 nm could be made to lase with an OC transmissivity T = 2.4%. Output power at each wavelength was 11 mW and 4 mW, whereas absorbed pump power threshold was 30 mW and 66 mW, respectively. The results are summarized in Fig. 12, with the output power and the threshold absorbed power predicted by the model. For comparison, the significantly larger gain of the Yb:YAG crystal allowed a relatively broad output wavelength tunability in CW regime using with the same OC, extending continuously from 1013 to 1070 nm, as shown in Fig. 13.

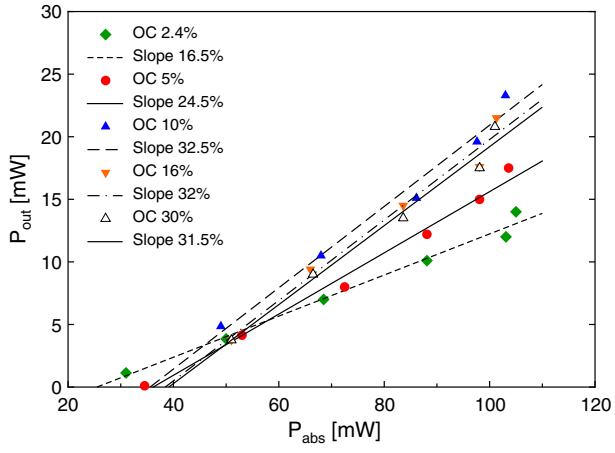

Fig. 8. CW operation of Yb:LuAG lasers with several output couplers.

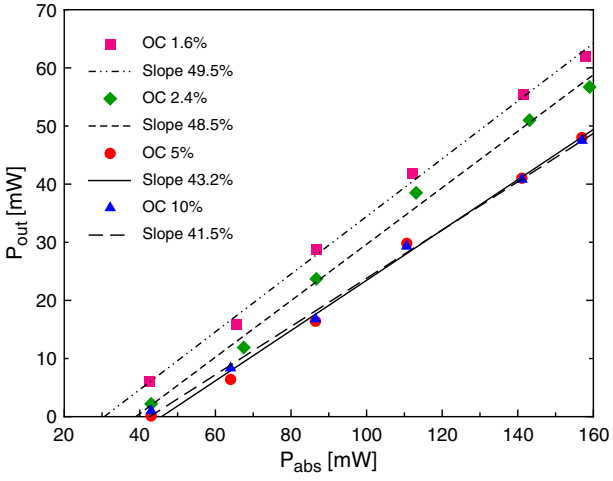

Fig. 9. CW operation of Yb:YAG lasers with several output couplers.

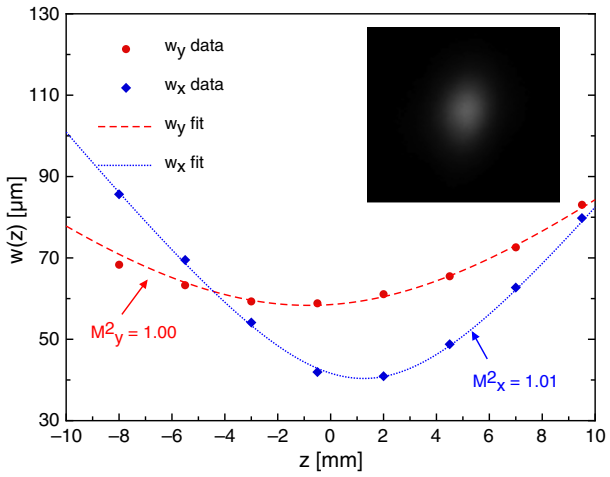

Fig. 10. Beam quality characterization results. In the inset a picture of the beam near the waist.

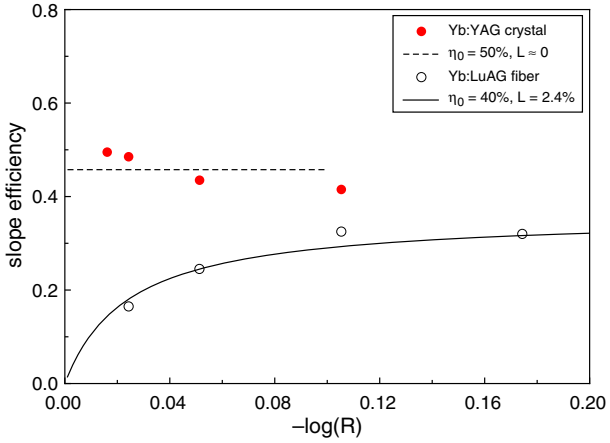

Fig. 11. Yb:YAG and Yb:LuAG slope efficiency as a function of output coupler mirror reflectivity. Also shown the results obtained by fitting the experimental data with Eq. (19).

This same model was applied to the Yb:LuAG experimental data, with larger quantitative disagreement even though the qualitative shape of the tuning curves is acceptable: this can be due to the lower pump power absorbed, that translates in laser operation closer to threshold, which makes laser alignment more critical and the optimization of the resonator performance more difficult in practice. For example, the tunable cavity for Yb:LuAG shows a significantly reduced output power compared to the Yb:YAG setup. Laser emission for Yb:LuAG grown by μ-PD technique has been obtained already [2], utilizing a sample with a

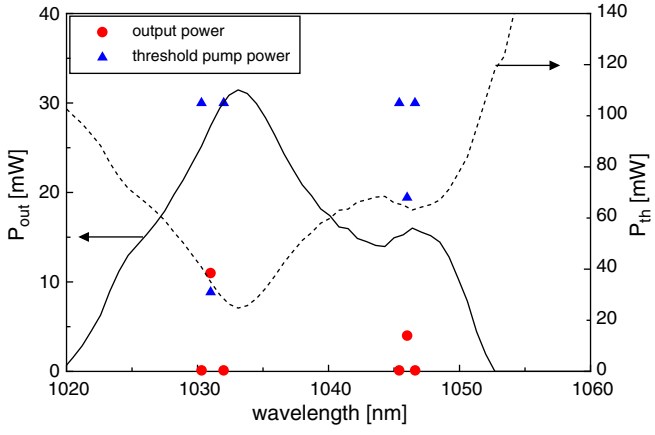

Fig. 12. Lasing wavelength tuning of Yb:LuAG sample with T = 2.4% output coupler.

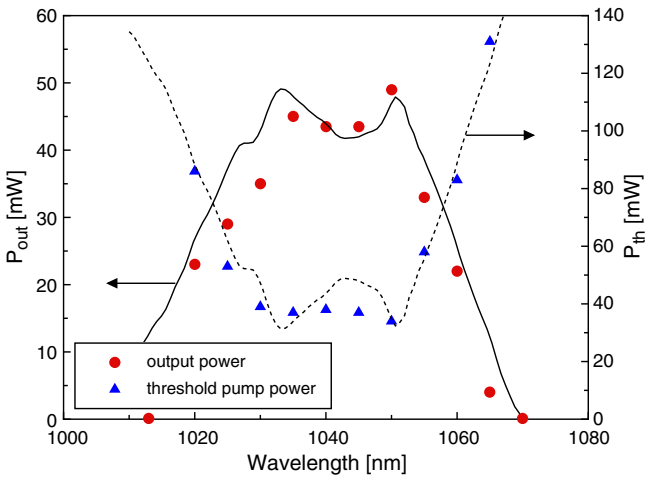

Fig. 13. Lasing wavelength tuning of Yb:YAG 1 mm thick, 10% doped sample with T = 2.4% output coupler.

doping level (0.9 at.%) close to that of our sample (1 at.%). The intrinsic slope efficiency $\eta_0 = 40\%$ measured in our experiment, quite comparable to that of the Yb:YAG reference ($\eta_0 = 50\%$) is a further proof of the good optical quality of the shaped rod crystal. The agreement of the scattering loss values measured in our work and in the report in Ref. [2] suggests that the much larger slope efficiency we measured (32% vs. 5%) is very likely due to much more effective pump mode matching, and in part to the use of a shorter crystal. Indeed, given the large output coupling used in high-power lasers (50% in Ref. [2]), the residual loss of relatively long fiber crystals ($\approx$50 mm) has a lesser impact, reducing the slope by a factor 0.7.

4. Conclusions

We have grown a LuAG:1 at.% Yb^{3+} shaped rod crystal, 130 mm length and 3 mm diameter. A sample of the shaped rod crystal has been optically characterized, recording an absorption spectrum at room temperature and performing fluorescence measurements as a function of temperature in the range 10–300 K. Lifetime of the $^2F_{5/2} \rightarrow {}^2F_{7/2}$ has been determined in the same temperature range. The absorption and emission cross sections have been calculated and utilized to evaluate the laser performances. A short Yb:LuAG laser crystal has been placed in an X cavity and pumped with a laser diode tuned at 935 nm. Laser experiments have shown that the Yb:LuAG sample grown by μ-PD technique appears to have an optical quality comparable with the largely utilized YAG. The laser performances are equivalent, considering the different doping level, to those obtained with a commercial YAG sample and a slope efficiency of 32% was obtained. This feature makes LuAG an appealing material for high power laser applications opening the way as well to obtain, by μ-PD technique, low cost and laser grade old and new materials.

References

[1] E.C. Honea, R.J. Beach, S.C. Mitchell, J.A. Skidmore, M.A. Emanuel, S.B. Sutton, S.A. Payne, P.V. Avizonis, R.S. Monroe, D.G. Harris, Fifteenth Topical Meeting of the Advanced Solid-State Lasers, Davos, Switzerland, February 13–16, 2000.
[2] D. Sangla, N. Aubry, A. Nehari, A. Brenier, O. Tillement, K. Lebbou, F. Balembois, P. Georges, D. Perrodin, J. Didierjean, J.M. Formigue, Journal of Crystal Growth 312 (2009) 125.
[3] N. Aubry, D. Sangla, C. Mancini, J. Didierjean, D. Perrodin, J.M. Formigue, O. Tillement, K. Lebbou, A. Brenier, C. Dujardin, F. Balembois, P. Georges, Journal of Crystal Growth 311 (2009) 4805.
[4] D. Maier, D. Rhede, R. Bertram, D. Klimm, R. Fornari, Optical Materials 30 (2007) 11.
[5] K.Y. Huang, K.Y. Hsu, D.Y. Jheng, W.J. Zhuo, P.Y. Chen, P.S. Yeh, S.L. Huang, Optics Express 16 (2008) 12264.
[6] A. Yoshikawa, V. Chani, MRS Bulletin 34 (2009) 266.

[7] Minh H. Pham, Marilou M. Cadatal, Toshihiro Tatsumi, Ayumi Saiki, Yusuke Furukawa, Tomoharu Nakazato, Elmer Estacio, Nobuhiko Sarukura, Toshihisa Suyama, Kentaro Fukuda, Kyoung Jin Kim, Yoshikawa Akira, Saito Fumio, Japanese Journal of Applied Physics 47 (2008) 5605.
[8] F. Euler, I.A. Bruce, Acta Crystallographica 19 (1965) 971.
[9] Brenier, et al., Journal of the Optical Society of America 23 (2006) 676.
[10] O. Kimmelma, I. Tittonen, S.C. Buchter, Applied Optics 47 (2008) 4262.
[11] A. Toncelli, M. Alshourbagy, M. Tonelli, Journal of Applied Physics 104 (2008) 104916.
[12] T.Y. Fan, R.L. Byer, IEEE Journal of Quantum Electronics 23 (1987) 605.
[13] W.P. Risk, Journal of the Optical Society of America B: Optical Physics 5 (1988) 1412.
[14] W. Koechner, Solid-State Laser Engineering, sixth ed. Springer Verlag, Heidelberg, 1999.